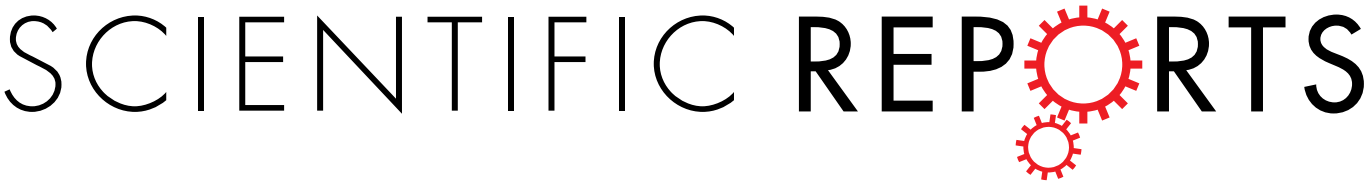

OPEN

Size-dependent electrical transport properties in Co nanocluster-assembled granular films

Received: 6 April 2017
Accepted: 24 August 2017
Published online: 15 September 2017

Q. F. Zhang, X. Z. Wang, L. S. Wang, H. F. Zheng, L. Lin, J. Xie, X. Liu, Y. L. Qiu, Y. Z. Chen & D. L. Peng

A series of Co nanocluster-assembled films with cluster sizes ranging from 4.5 nm to 14.7 nm were prepared by the plasma-gas-condensation method. The size-dependent electrical transport properties were systematically investigated. Both of the longitudinal resistivity (ρ_{xx}) and saturated anomalous Hall resistivity (ρ_{xy}^{A}) continuously increased with the decrease of the cluster sizes (d). The ρ_{xx} firstly increased and then decreased with increasing the temperature for all samples, which could be well described by involving the thermally fluctuation-induced tunneling (FIT) process and scattering. The tunneling effect was verified to result in the invalidation of classical anomalous Hall effect (AHE) scaling relation. After deducting the contribution from tunneling effect to ρ_{xx}, the AHE scaling relation between ρ_{xy}^{A} and the scattering resistivity (ρ_{S}) by varying the temperature was reconstructed. The value of scaling exponent γ increased with increasing Co cluster sizes. The size dependence of γ might be qualitatively interpreted by the interface and surface-induced spin flip scattering. We also determined the scaling relation between ρ_{xy}^{A} and ρ_{S} at 5 K by changing the Co cluster sizes, and a large value of $\gamma = 3.6$ was obtained which might be ascribed to the surface and interfacial scattering.

Magnetic granular film, as a class of functional materials, is very attractive due to its rich fundamental phenomena and opening a new route for potential novel applications[1–3]. The AHE in ferromagnets, arising from several origins, is one of the most prominent phenomena. For the present theories in homogeneous magnetic materials, it is generally accepted that the skew scattering ($\gamma = 1$)[4], side-jump ($\gamma = 2$)[5], and intrinsic ($\gamma = 2$)[6] mechanisms account for the AHE, which gives an expression of $\rho_{xy}^{A} \propto \rho_{xx}^{\gamma}$. Therefore, one can parse the microscopic mechanisms of AHE by determining the scaling relation experimentally. However, large number of the theoretical and experimental results revealed that the AHE scaling relation in heterogeneous material was counterintuitive, especially in multilayer film and granular film[7–9]. Song *et al.* studied the AHE in Fe/Cr multilayers and observed a large scaling exponent ($\gamma = 2.6$) which resulted from the interfacial scattering[8]. Guo *et al.* discovered a large scaling exponent in Co/Pd multilayer films ($\gamma = 5.7$) which was also ascribed to the interfacial scattering[10]. In addition, Zhang *et al.* observed a large enhancement of ρ_{xy}^{A} in Co/Pt multilayers by inserting the MgO/CoO hybrid bilayers[11]. Afterwards, Guo *et al.* also obtained a large enhancement of ρ_{xy}^{A} in Co/Pd multilayers by modifying the interfacial structures[12]. These results gave a strong indication that the interfacial scattering could significantly enhance the AHE. The AHE in granular films also have received extensive attention because of their abundant surface/interface and controllable microstructure[13–15]. The microstructure in granular films can be effectively adjusted by governing the experiment parameters. Xiong *et al.* studied the size dependence of ρ_{xy}^{A} and ρ_{xx} in Co-Ag granular films by changing the annealing temperature, and the scaling exponent of $\gamma = 3.7$ was obtained at 4.2 K[9]. They also found that the ρ_{xy}^{A} increased with the decrease of Co grain sizes. The size dependence of ρ_{xy}^{A} was also observed in Co-Cu granular films[16]. These experimental observations implied that the grain size had a crucial effect on AHE. Nevertheless, the annealing affected the microstructure of the granular system by a complicated way[17]. In this case, it was difficult to accurately demarcate the contribution of grain size, interface and interparticle distance to AHE. In the aspects of theoretical research, Granovsky *et al.*[18] and Vedyaev *et al.*[19] also suggested that the decrease of the grain sizes would effectively improve the ρ_{xy}^{A} and the value of γ displayed obvious

Department of Materials Science and Engineering, Collaborative Innovation Center of Chemistry for Energy Materials, College of Materials, Xiamen University, Xiamen, 361005, China. Correspondence and requests for materials should be addressed to L.S.W. (email: wangls@xmu.edu.cn) or D.L.P. (email: dlpeng@xmu.edu.cn)

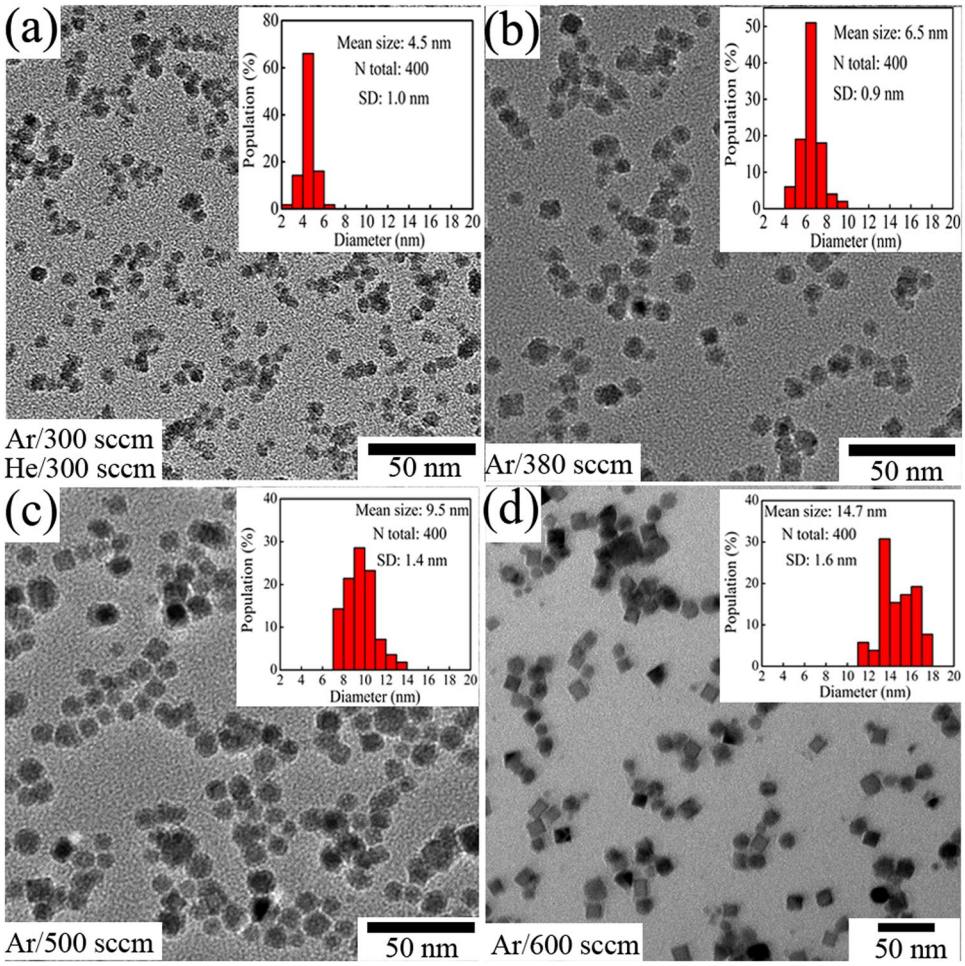

Figure 1. (**a**–**d**) Low-magnification TEM images of Co nanoclusters with different size. The inset in (**a**–**d**) are the corresponding size distribution.

size-dependent in granular films. Unfortunately, the experimental evidence is still very scarce. The most critical factor is that it is difficult to individually control the grain size and interparticle distance by conventional preparation techniques. In this case, the size-dependent AHE remains an open question. Consequently, it is necessary and interesting to develop a more effective preparation method and study the size-dependent AHE in uniform single phase magnetic granular system.

In this paper, the uniform Co nanocluster-assembled granular films with different Co cluster sizes by plasma-gas-condensation (PGC)-type cluster beam deposition apparatus. With this method, we successfully realized the individual control of cluster size. And then we systematically studied the Co cluster sizes dependence of ρ_{xx} and ρ_{xy}^{A} in uniform Co nanocluster-assembled films. Both of the ρ_{xx} and ρ_{xy}^{A} increased with the decrease of cluster sizes which could be attributed to the increase of surface and interfacial scattering. Furthermore, the size-dependent γ were investigated and corresponding physical mechanisms were discussed. Our results provide unequivocal experimental evidences for the effect of cluster size on the AHE.

Results and Discussion

The Low-magnification TEM images and the corresponding size distribution of the Co nanoclusters are displayed in Fig. 1. The statistical results showed that the average size of clusters decreased from 14.7 nm to 6.5 nm as the Ar flow rate reduced from 600 sccm to 380 sccm, and further decreased to 4.5 nm when the 300 sccm He and 300 sccm Ar were simultaneously injected into deposition chamber [Fig. 1(a)]. The narrow size distribution meant that the size of Co clusters for all samples were very uniform. Additionally, the Co clusters were almost cubic geometry at $d = 14.7$ nm while gradually turned into spherical-like with the decrease of Co cluster sizes due to the high-surface-energy and small size effect. Hence, the size and geometry of Co clusters could be adjusted by tuning the Ar and He flow rates.

Figure 2(a) displays the SAED pattern of Co nanocluster-assembled film for $d = 14.7$ nm. The diffraction rings 2, 3, 5 and 6 corresponded to the {111}, {200}, {220} and {311} planes of metastable fcc Co. The presence of the diffraction rings 1 and 4 were attributed to {111} and {220} planes of fcc CoO, which was possibly originated from slight oxidization when the samples were exposed to the ambient atmosphere. The high-resolution TEM observation of the Co clusters is exhibited in Fig. 2(b). The lattice fringe of 0.205 nm belonged to {111}

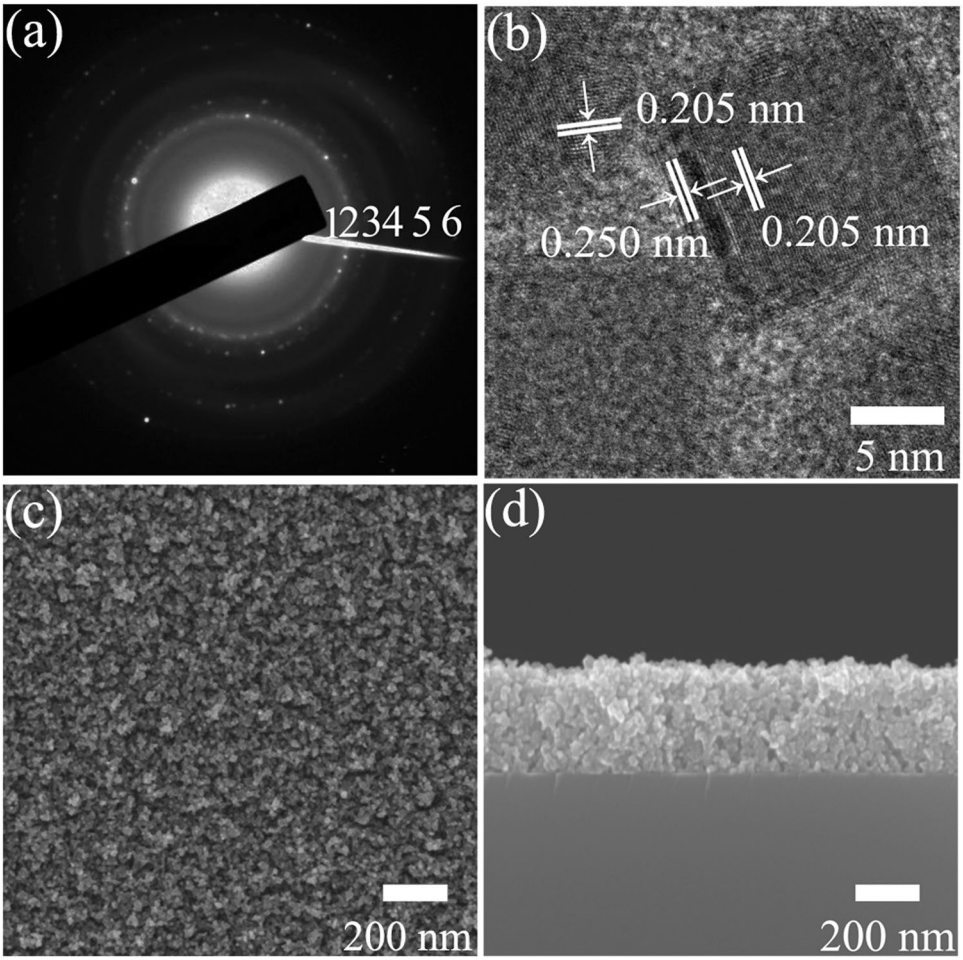

Figure 2. (**a**) SAED pattern, (**b**) high-resolution TEM image, (**c**) plan-view and (**d**) cross-sectional SEM images of the Co nanocluster-assembled film for $d = 14.7$ nm.

interplanar spacing of metastable fcc Co. While the lattice fringes of 0.250 nm corresponded to {111} interplanar spacing of fcc CoO, which agreed well with the observation in Fig. 2(a). The adjacent Co clusters connected with each other, forming three-dimensional (3D) effective conductive paths. Figure 2(c-d) show the planar-view and cross-sectional SEM images of the Co cluster-assembled film for $d = 14.7$ nm. These results demonstrated that a porous structure and the randomly stacking of the Co cluster were obtained in granular films.

Figure 3 plots the variation in ρ_{xx} with the temperature for the four representative samples. In all cases, the ρ_{xx} first decreased and then increased with the increase of temperature, resulting in a minimum value at a certain temperature (T_{min}). In the high temperature region ($T > T_{min}$), all samples exhibited a positive temperature coefficient of resistance (TCR). Nevertheless, a negative TCR was observed in the low temperature range ($T < T_{min}$). It was worth mentioning that the atom distribution at the Co clusters surface and interface was highly disorder and slightly oxidized [Fig. 2(a-b)]. In this case, the interface between adjacent Co clusters could be considered as mesoscopic tunnel junctions and the barrier height was low enough. Under the circumstances, the negative TCR observed in our samples could be attributed to tunneling effect suggested by FIT process[20,21]. As can be seen from Fig. 3(d), the value of ρ_{xx} for $d = 14.7$ nm at 300 K was far larger than the reported value in Co epitaxial thin films[22], which was attributed to the strong surface/interfacial scattering and tunneling effect in our sample. Guo *et al*. studied the electrical transport properties in polycrystalline Ni films and suggested that the total resistivity could be written as the superposition of tunneling effect and scattering[23]. Hence, the temperature-dependent ρ_{xx} in our samples might also be given as:

$$\rho_{xx} = \rho_0 \exp\left(\frac{T_1}{T + T_0}\right) + BT^2 + CT^3 + DT^5. \quad (1)$$

Here, the first term represents the resistivity dominated by FIT process and the residual terms are the contribution from temperature-dependent scattering[21,24–26]. The T^2 term includes the contribution from magnetic scattering, surface-induced scattering, and electron-electron scattering. The T^3 and T^5 terms are mainly ascribed to the contribution from phonon scattering in the framework of the Bloch-Wilson and Bloch-Gr€uneisen formula,

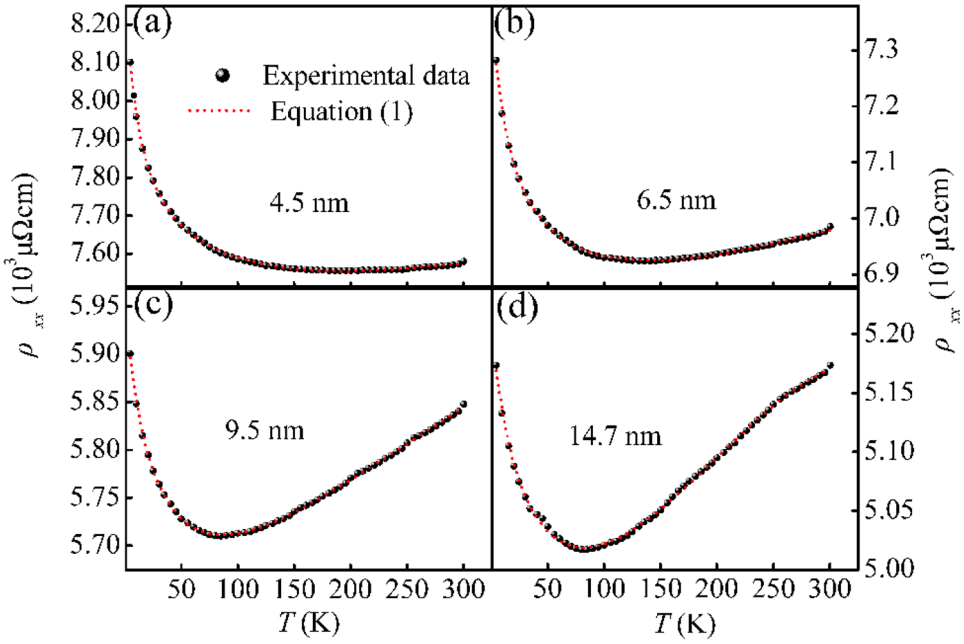

Figure 3. $\rho_{xx} - T$ curves for Co nanocluster-assembled films with different Co cluster sizes. The symbols are the experimental data. The short dash curves are the theoretical forecasting by Eq. (1).

d (nm)	T_1 (K)	T_0 (K)	T_1/T_0
4.5	1.539	15.108	0.102
6.5	1.526	19.111	0.080
9.5	1.566	25.128	0.062
14.7	1.876	37.404	0.050

Table 1. Data for the fitting parameters attained from Eq. (1).

respectively[21]. The coefficient of B, C, D and ρ_0 are constant. T_1 and T_0 are characteristic parameters depending on mesoscopic tunnel junctions, which can be further expressed as[20]:

$$T_1 = \frac{8\varepsilon_0 A V_0^2}{e^2 k_B \omega}, \tag{2}$$

and

$$T_0 = \frac{16\varepsilon_0 \hbar A V_0^{3/2}}{\pi e^2 k_B \omega^2 \sqrt{2m}}. \tag{3}$$

Here, ω is the junction width, A is the junction area, and V_0 is the barrier height (See Supplementary Fig. S1). m represents the electronic mass, ε_0 is the permittivity of vacuum and $\hbar$ is reduced Planck's constant. As can be seen from Fig. 3, the experimental results for all samples agreed well with the theoretically predicted by Eq. (1). This gave a clear indication that the ρ_{xx} originated form the superposition of tunneling effect and scattering, and scattering dominated the ρ_{xx} in the high temperature range, while FIT process gradually became important with the decrease of temperature. The fitting parameters are displayed in Table 1.

To further clarify the physical mechanism in Co nanocluster-assembled granular films, we reconstructed the Eqs (2) and (3). The expression of $T_1/T_0 \propto \omega V_0^{1/2}$ was obtained. According to the definition in FIT model, the decay length of the tunneling electron wave function inside the barrier is given as $\xi = \hbar/\sqrt{2mV_0}$. Hence, the T_1/T_0 can be further written as $T_1/T_0 \propto \omega/\xi$. This signifies that a lower value of T_1/T_0 corresponds to a higher electron tunneling probability. As can be seen from Table 1, the value of T_1/T_0 decreased with increasing the Co cluster sizes, suggesting a higher electron tunneling probability between adjacent Co clusters. Such a behavior revealed that the contribution from tunneling effect decreased with increasing Co cluster sizes. Meanwhile, a higher electron tunneling probability indicated a lower barrier height at interface between adjacent Co clusters. This scenario revealed that the atom distribution disorder at interface decreased with the increase of Co cluster sizes. On the other hand, the number of Co clusters in unit volume deceased with the increasing Co cluster sizes. Hence, the amount of the interface and surface in in unit volume also deceased with the increase of Co cluster sizes,

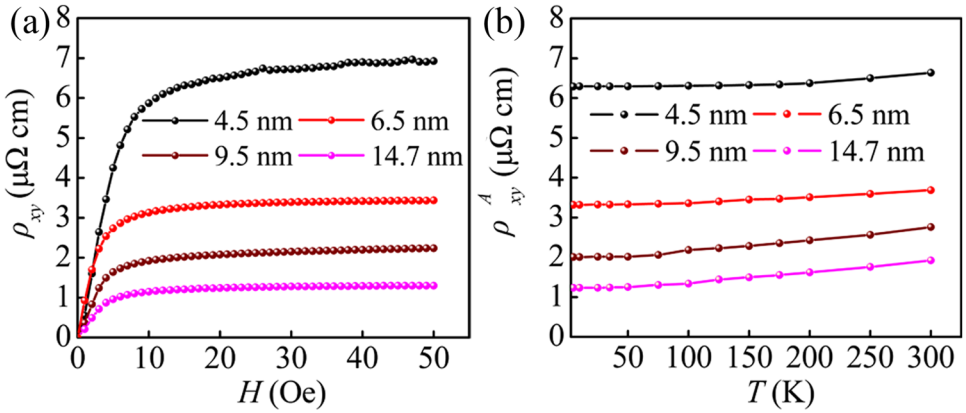

Figure 4. (**a**) The Hall resistivity as a function of field at 5 K, and (**b**) $\rho_{xy}^{A} - T$ curves for the Co nanocluster-assembled films with different Co cluster sizes.

suggesting the decrease of interfacial and surface scattering. Hence, the ρ_{xx} decreased monotonously with the increase of Co cluster sizes might mainly result from the less contribution from FIT process, interfacial and surface scattering.

The field-dependent Hall resistivity ρ_{xy} for all the samples at 5 K are plotted in Fig. 4(a). Generally, the Hall resistivity is parameterized by $\rho_{xy} = \rho_{xy}^{O} + \rho_{xy}^{A} = R_0 H + 4\pi R_S M$[27]. R_0, R_s and M are defined as ordinary Hall coefficient, anomalous Hall coefficient and magnetization, respectively. As shown in Fig. 4(a), the ρ_{xy} sharply increased at low fields and gradually tended to saturation at high fields. The R_S could be achieved by mathematical calculation based on the above-mentioned definition formulas of ρ_{xy} and the magnetization curves data (See Supplementary Fig. S2). The calculation results of R_S at 300 K were 1.06×10^{-8} (Ω cm)/G, 3.37×10^{-9} (Ω cm)/G, 1.79×10^{-9} (Ω cm)/G and 1.15×10^{-9} (Ω cm)/G for 4.5 nm, 6.5 nm, 9.5 nm and 14.7 nm, respectively. It is worth noting that, the value of R_S for 4.5 nm Co granular film was almost four orders of magnitude larger than the reported value in blocky single-crystal Co[28]. Such a significant enhancement of Hall coefficient was closely related to large amount of interface and surface. The saturate anomalous Hall resistivity was acquired by using $\rho_{xy}^{A} = 4\pi R_S M$ at $H = 5$ T (M was measured by Quantum Design physical property measurement system). Referring to this method, the ρ_{xy}^{A} with different temperature for the four representative samples are obtained and display in Fig. 4(b). It can be seen form this figure that the value of ρ_{xy}^{A} increased continuously with increasing the temperature. Such a behavior was mainly ascribed to surface and interfacial scattering[21]. However, based on the current experimental data, the contribution of intrinsic mechanism could not be ruled out. This behavior was well supported by the results in Co/Pd multilayers[10]. Pay attention to this figure, the ρ_{xy}^{A} increased monotonously with the decrease of Co cluster sizes. This was because, as mentioned above, the atom distribution disorder at surface and interface increased with the decrease of Co cluster sizes. It is well known that the AHE was closely related to spin-orbit scattering of conduction electrons at disorder sites in ferromagnet[29,30]. In the Co nanocluster-assembled films, the amount of surface and interface increased with decreasing Co cluster sizes. These behaviors would effectively enhance the amount of scattering center in the samples. Therefore, the increase of the spin-orbit scattering finally enhanced the ρ_{xy}^{A}. Such a behavior was supported by the observation in Co/Pd multilayers[12] and Fe nanocluster-assembled films[31], which also indicated that surface and interfacial scattering made a significant contribution to improve the AHE. Moreover, this result provided an experimental evidence for the theoretic investigation from Granovsky *et al.*[18] and Vedyaev *et al.*[19].

To further identify the AHE mechanism in Co nanocluster-assembled films, the ρ_{xy}^{A} and ρ_{xx} were compiled into a power law of $\rho_{xy}^{A} \propto \rho_{xx}^{\gamma}$. Figure 5(a) shows the scaling behavior of ρ_{xy}^{A} vs ρ_{xx} with different Co cluster sizes. It was clear that two distinct regions were observed in $\log\rho_{xy}^{A}$ varying with $\log\rho_{xx}$ for all samples and the demarcation point was the resistivity of T_{min}. Fitting the data into straight line, a negative γ was observed in the temperature range $T < T_{min}$, while a positive γ was found at higher temperature region ($T > T_{min}$). The corresponding γ are exhibited in Fig. 5(b). Unfortunately, both of the negative and positive γ in our samples could not be explained by classical AHE scaling theory. Moreover, the value of γ clearly depended on the Co cluster size. There were some works indicated that the ρ_{xx} and ρ_{xy}^{A} dominated by different physical mechanisms and the tunneling effect had little effect on AHE[32,33]. It should be noted that the tunneling effect worked in the whole temperature range. Especially in the temperature range $T < T_{min}$, the ρ_{xx} was principally governed by tunneling effect. Therefore, it was no wonder that the classical scaling relation between ρ_{xy}^{A} and ρ_{xx} was invalid in our systems even in higher temperature range ($T > T_{min}$). To gain insight into the physical mechanisms of AHE in Co nanocluster-assembled films, tunneling effect should be removed from ρ_{xx}, and the scaling relation between ρ_{xy}^{A} and the resistivity only deriving from scattering should be reconsidered.

It was worth mentioning that, as the temperature increased to be in a high limit, the tunneling effect can be neglected. In this case, the resistivity was only originated from scattering. Hence, the Eq. (1) can be rewritten

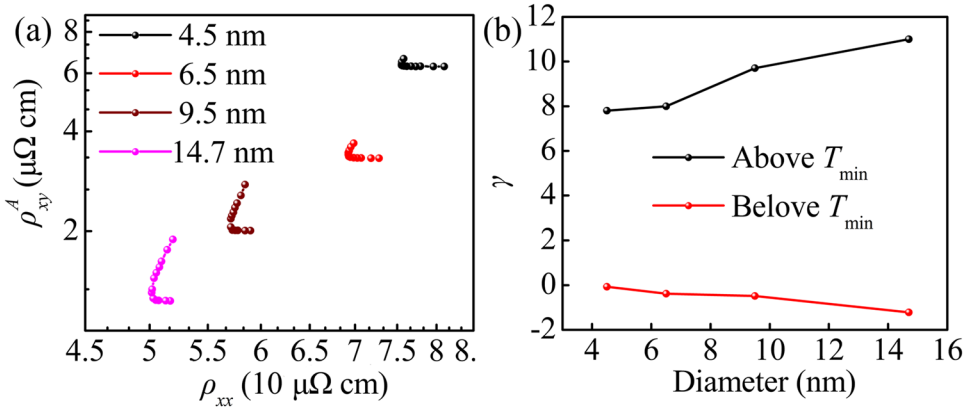

Figure 5. (**a**) The $\log\rho_{xy}^{A} - \log\rho_{xx}$ curves for the Co nanocluster-assembled films with different Co cluster sizes. (**b**) The corresponding scaling exponent of AHE.

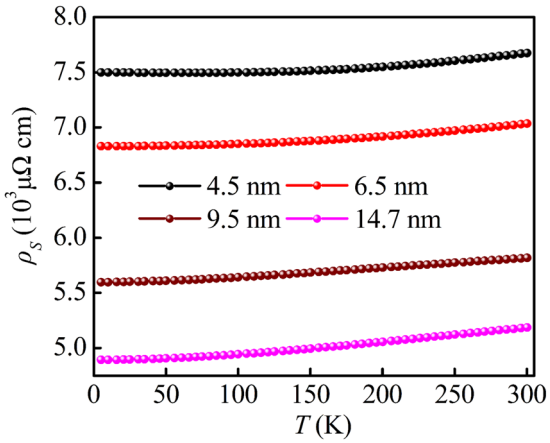

Figure 6. $\rho_S - T$ curves for the Co nanocluster-assembled films with different Co cluster sizes.

as $\rho_{xx(T\to\infty)} = \rho_0 + \rho_{ST}$. Here, ρ_{ST} is the temperature-dependent resistivity, which is given as $\rho_{ST} = BT^2 + CT^3 + DT^5$. ρ_0 is equivalent to residual resistivity which was originated from impurity or imperfection scattering. The scattering resistivity ρ_S including residual resistivity ρ_0 and temperature-dependent scattering resistivity can be written as:

$$\rho_S = \rho_0 + \rho_{ST} = \rho_0 + BT^2 + CT^3 + DT^5 \quad (4)$$

According to the fitting parameters from Eq. (1), we could effectively evaluate the contribution from ρ_0 and temperature-dependent scattering (ρ_{ST}). In this case, the scattering resistivity with different temperature could be obtained. The $\rho_S - T$ curves with different Co cluster sizes are shown in Fig. 6. Different from the measuring results in Fig. 3, the ρ_S for all samples continuously increased with increasing the temperature, indicating a behavior of a normal metal conduction characteristic. Moreover, the ρ_S increased monotonically with decreasing Co cluster sizes. The phenomenon agreed well with the result presented in Fig. 4(b), which was ascribed to the increase of surface and interfacial scattering because of the raise of the amount of scattering center.

The AHE scaling between ρ_{xy}^{A} and ρ_S with different Co cluster sizes are exhibited in Fig. 7(a). Remarkably different from the observation in Fig. 5(a), the $\log\rho_{xy}^{A}$ increased monotonously with increasing $\log\rho_S$ in the whole temperature range. This observation gave an unambiguous indication that after deducting the contribution from tunneling effect the scaling relation was constructed successfully. By fitting the data to a straight line, the positive scaling exponent for all samples were observed but all of γ were larger than 2. The large scaling exponent observed in our samples could be qualitatively attributed to surface and interfacial scattering. The present results agreed with the previously reported in some other heterogeneous systems, such as Fe/Cr multilayers ($\gamma = 2.6$)[8], ε-Fe_3N nanocrystalline films ($\gamma = 17.6$)[34] and Fe/Au multilayers ($\gamma = 2.7$)[35]. More importantly, as shown in Fig. 7(b), the scaling exponent γ increased with increasing Co cluster sizes. To some extent, the γ could be considered as a quantified criterion to evaluate how fast the ρ_{xy}^{A} increased with the raise of ρ_S. In our samples, both of the ρ_{xy}^{A} and ρ_S approximately originated from three parts: bulk scattering, interface scattering and surface scattering[21].

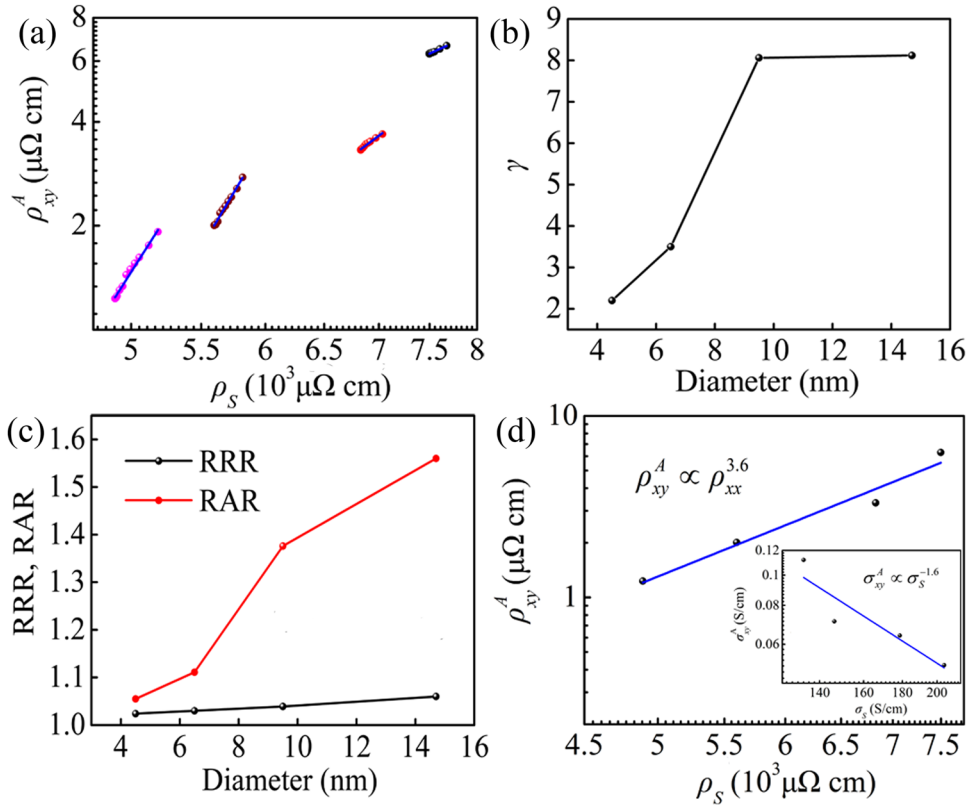

Figure 7. (**a**) The plot of $\log\rho_{xy}^{A} - \log\rho_S$ curves for the Co nanocluster-assembled films with different sizes. (**b**) The scaling exponent, (**c**) the RRR and RAR as function of Co cluster sizes. (**d**) The $\log\rho_{xy}^{A} - \log\rho_S$ curve at 5 K. The inset shows the scaling of the σ_{xy}^{A} becomes σ_{xx}.

According to the previous report in Co epitaxial thin films[22], the contribution from bulk scattering was independent on thickness of film. Unlike the Co epitaxial film, there was lager amount of surface and interface in our samples, which would introduce additional scattering center. On the one hand, as mentioned above, the increasing scattering center would effectively increase both of the ρ_{xy}^{A} and ρ_S. On the other hand, great scattering strength could cause the spin flip to randomize the spins[10,36,37], which would effectively reduce the spin-dependent scattering ratio but had a limited impact on ρ_S. To gain a deeper understanding of this behavior, the residual resistivity ratio [RRR = ρ_S(300 K)/ρ_S(5 K)] of all samples was studied. The RRR is considered as a qualitative method to identify degree of atomic disorder and lattice defect[38]. It should be noted that, at 5 K, the contribution from temperature-dependent scattering could be nearly neglected. In this case, the scattering resistivity was approximately equivalent to residual resistivity [ρ_S(5K) ≈ ρ_0]. In analogy with RRR, we defined the residual saturate anomalous Hall resistivity ratio as RAR = ρ_{xy}^{A}(300 K)/ρ_{xy}^{A}(5 K). The size dependence of RRR and RAR are displayed in Fig. 7(c). Obliviously, the values of RRR decreased with the drop of Co nanocluster sizes, suggesting the improvement of degree of atomic disorder and lattice defect with decreasing cluster size. This conclusion reconfirmed the result mentioned above (T_1/T_0). Furthermore, it was obvious that RAR shown a sharper decrease than RRR with the decrease of Co cluster sizes. This indicated that temperature-dependent ρ_{xy}^{A} and ρ_S were affected by different physical mechanisms, and the spin flip enhanced at high density of interface and surface. As a consequence, the size-dependent γ in the Co nanocluster-assembled films might be qualitatively interpreted by the enhancement of interface and surface-induced spin flip to randomize the spins. Such a behavior was in good accord with the experimental investigation in Co/Pd multilayers[10] and the theoretical research from Granovsky *et al.*[18] and Vedyaev *et al.*[19].

Nagaosa *et al.* proposed that the more proper test of the scaling relation was at low temperature by varying the defect concentration where the resistivity was dominated by impurity scattering because the interference from temperature-dependent-scattering could be excluded[27]. Hence, in order to further clarify the physical mechanism of AHE in our samples, we should exclude the effect from temperature-dependent-scattering and tunneling effect and tested the scaling relation between ρ_S and ρ_{xy}^{A} at low temperature. The $\log\rho_{xy}^{A} - \log\rho_S$ curve at 5 K is plotted [Fig. 7(d)]. The $\log\rho_{xy}^{A}$ increased monotonically with the increase of $\log\rho_S$, which followed a linear behavior. Carrying on the data fitting to the experimental results, the scaling exponent $\gamma = 3.6 \pm 0.4$ was observed. Therefore, the value of $\gamma = 3.6 \pm 0.4$ was related to surface and interfacial scattering. Recently, another interesting finding was that Nagaosa *et al.*[27] proposed the unified theory of the AHE based on a large body of experimental results and theoretical study. The theory predicted that three broad regimes were distinguished as a function

of longitudinal conductivity (σ_{xx}). (i) $\sigma_{xx} > 10^6$ S/cm (high conductivity regime), skew scattering mechanism dominates the Hall transport. (ii) 10^4 S/cm $< \sigma_{xx} < 10^6$ S/cm (intrinsic regime) in which anomalous Hall conductivity σ_{xy}^A becomes σ_{xx} independent. (iii) $\sigma_{xx} < 10^4$ S/cm (bad metal regime), where $\sigma_{xy}^A \propto \sigma_{xx}^{1.6}$ is predicted. The value of the σ_{xy}^A and σ_{xx} are estimated separately by $\sigma_{xy}^A \approx \rho_{xy}^A/\rho_{xx}^2$ and $\sigma_{xx} \approx 1/\rho_{xx}$ because of $\rho_{xy}^A << \rho_{xx}$. As shown in the inset of Fig. 7(d), apparently, all of our samples were in the bad metal regime. Fitting the experimental data into a straight line, $\sigma_{xy}^A \propto \sigma_S^{-1.6}$ was obtained at 5 K (σ_S represented the longitudinal conductivity originating from scattering), which disagreed with the universal character of the 1.6 scaling relation. This result gave a strong indication that our samples was inconsistent with the unified theory, which was mainly ascribed to the surface and interfacial scattering. The similar phenomenon also could be observed in ε-Fe_3N nanocrystalline films[34].

In summary, the uniform Co nanocluster-assembled films with different Co cluster sizes were successfully prepared by the plasma-gas-condensation method. For all samples, the longitudinal resistivity could be very well fitted by the combination of FIT process and scattering in the whole temperature range. Both of ρ_{xx} and ρ_{xy}^A shown a decreasing function of the Co cluster sizes due to the drop of surface and interfacial scattering. The scaling relation of $\rho_{xy}^A \propto \rho_{xx}^\gamma$ could be divided into two parts while obeyed the same line relationship between ρ_{xy}^A and ρ_S in the whole temperature range, indicating that it was necessary to remove the tunneling effect in establishing the AHE scaling relation. The large scaling exponent ($\gamma > 2$) observed in our samples could be ascribed to the surface and interfacial scattering and the size-dependent scaling exponent were closely related to the interface and surface-induced spin flip scattering. The large anomalous Hall coefficient [$R_s \sim 1.06 \times 10^{-8}$ (Ω cm)/G] observed $d = 4.5$ nm could be attributed to the large amount of surface and interface, which is especially valuable in practical application in Hall device applications.

Methods

The experimental apparatus of plasma-gas-condensation (PGC)-type cluster deposition system was employed to prepare the samples. The apparatus was simply divided into three regions: a sputtering chamber, a cluster growth room and a deposition chamber[39]. The nucleation and growth of Co clusters occurred mainly in the sputtering chamber. And then Co clusters were extracted twice in the cluster growth room to prevent further growth. Finally, the Co clusters entered into the deposition chamber and softly deposited onto substrate randomly. The DC power of 400 W was used to generate high density metal Co vapor. The argon gas (99.999%) and helium gas (99.999%) with different flow rates (Ar: 600 sccm, Ar: 500 sccm, Ar: 400 sccm, and Ar/He: 300 sccm/300 sccm) were injected continuously into sputtering chamber to control the Co cluster sizes. JEOL JEM-2100 transmission electron microscope (TEM) was used to carry out transmission electron microscopy (TEM) analysis. The morphology and crystalline phase of Co clusters were determined by TEM images and the selected area electron diffraction (SAED) was used to identify crystalline phase. The surface micro-morphology images of Co clusters-assembled films were acquired by SU-70 scanning electron microscope (SEM). The magnetic and electrical properties were performed on Quantum Design physical property measurement system (PPMS-9) with temperatures ranging from 5 to 300 K and the magnetic field sweeping from −5 to 5 T. For each sample, the longitudinal and transverse voltage could be measured simultaneously because of the five contacts in Hall bar. The thickness of cluster-assembled films (~700 nm) were determined by the surface profiler (Alpha-Step D-100).

References

1. Chadha, M. & Ng, V. Sequential sputtered Co-HfO_2 granular films. *J. Magn. Magn. Mater* **426**, 302 (2017).
2. Sonntag, J. The Origin of the Giant Hall Effect in Metal-Insulator Composites. *Open Journal of Composite Materials* **6**, 78 (2016).
3. Bartov, D., Segal, A., Karpovski, M. & Gerber, A. Absence of the ordinary and extraordinary Hall effects scaling in granular ferromagnets at metal-insulator transition. *Phys. Rev. B* **90**, 144423 (2014).
4. Smit, J. The spontaneous Hall effect in ferromagnetics I. *Physica* **21**, 877 (1955).
5. Berger, L. Side-jump mechanism for the Hall effect of ferromagnets. *Phys. Rev. B* **2**, 4559 (1970).
6. Karplus, R. & Luttinger, J. M. Hall Effect in Ferromagnetics. *Phys. Rev.* **95**, 1154 (1954).
7. Canedy, C. L., Li, X. W. & Xiao, G. Large magnetic moment enhancement and extraordinary Hall effect in Co/Pt superlattices. *Phys. Rev. B* **62**, 508 (2000).
8. Song, S. N., Sellers, C. & Ketterson, J. B. Anomalous Hall effect in (110) Fe/(110) Cr multilayers. *Appl. Phys. Lett.* **59**, 479 (1991).
9. Xiong, P. *et al*. Extraordinary Hall effect and giant magnetoresistance in the granular Co-Ag system. *Phys. Rev. Lett.* **69**, 3220 (1992).
10. Guo, Z. B. *et al*. Effects of surface and interface scattering on anomalous Hall effect in Co/Pd multilayers. *Phys. Rev. B* **86**, 104433 (2012).
11. Zhang, J. Y. *et al*. Effect of interfacial structures on anomalous Hall behavior in perpendicular Co/Pt multilayers. *Appl. Phys. Lett.* **102**, 102404 (2013).
12. Guo, Z. B., Mi, W. B., Li, J. Q., Cheng, Y. C. & Zhang, X. X. Enhancement in anomalous Hall resistivity of Co/Pd multilayer and CoPd alloy by Ga^+ ion irradiation. *Europhys. Lett.* **105**, 46005 (2014).
13. Wang, J. B., Mi, W. B., Wang, L. S., Zhang, Q. F. & Peng, D. L. Enhanced anomalous Hall effect in Fe nanocluster assembled thin films. *Phys. Chem. Chem. Phys.* **16**, 16623 (2014).
14. Wang, J. B. *et al*. Anomalous Hall effect in monodisperse CoO-coated Co nanocluster-assembled films. *J. Magn. Magn. Mater.* **401**, 30 (2016).
15. Li, H. B. *et al*. Extraordinary Hall effect and universal scaling in $Fe_x(ZnO)_{1-x}$ granular thin films at room temperature. *Appl. Phys. Lett.* **106**, 012401 (2015).
16. Wang, J. Q. & Kim, H. K. Effect of Annealing on Extraordinary Hall Effects in Sputtered Granular $Cu_{80}Co_{20}$ Thin Films. *IEEE T. Magn.* **42**, 3282 (2006).
17. Gerber, A. *et al*. Correlation between the extraordinary Hall effect and resistivity. *Phys. Rev. B* **69**, 224403 (2004).
18. Granovsky, A., Brouers, F., Kalitsov, A. & Chshiev, M. Extraordinary Hall effect in magnetic granular alloys. *J. Magn. Magn. Mater.* **166**, 193 (1997).
19. Vedyaev, A. V., Granovskii, A. B., Kalitsov, A. V. & Brouers, F. Anomalous Hall effect in granular alloys. *JETP* **85**, 1204 (1997).
20. Sheng, P. Fluctuation-induced tunneling conduction in disordered materials. *Phys. Rev. B* **21**, 2180 (1980).
21. Zhang, Q. F. *et al*. Electrical transport properties in Co nanocluster-assembled granular film. *J. Appl. Phys.* **121**, 103901 (2017).
22. Hou, D. Z. *et al*. The anomalous Hall effect in epitaxial face-centered-cubic cobalt films. *J. Phys. Condens. Matter* **24**, 482001 (2012).
23. Guo, Z. B. *et al*. Anomalous Hall effect in polycrystalline Ni films. *Solid State Communications* **152**, 220 (2012).

24. Kamalakar, M. V., Raychaudhuri, A. K., Wei, X. Y., Teng, J. & Prewett, P. D. Temperature dependent electrical resistivity of a single strand of ferromagnetic single crystalline nanowire. *Appl. Phys. Lett.* **95**, 013112 (2009).
25. Zhang, P., Cohen, R. E. & Haule, K. Effects of electron correlations on transport properties of iron at Earth's core conditions. *Nature* **517**, 605 (2015).
26. Lal, K. *et al.* A low temperature study of electron transport properties of tantalum nitride thin films prepared by ion beam assisted deposition. *Solid State Commun* **131**, 1 (2004).
27. Nagaosa, N., Sinova, J., Onoda, S., MacDonald, A. H. & Ong, N. P. Anomalous hall effect. *Rev. Mod. Phys.* **82**, 1539 (2010).
28. Kondorskii, E. N., Galkina, O. S., Ivanovskii, V. I., Cheremushkina, A. V. & Usarov, U. T. Anisotropy of galvanomagnetic effects in single-crystal cobalt. *Sov. Phys. JETP* **38**, 977 (1974).
29. Wu, S. B., Yang, X. F., Chen, S. & Zhu, T. Scaling of the anomalous Hall effect in perpendicular CoFeB/Pt multilayers. *J. Appl. Phys.* **113**, 17C119 (2013).
30. Zhang, J. Y. *et al.* Effect of MgO/Co interface and Co/MgO interface on the spin dependent transport in perpendicular Co/Pt multilayers. *J. Appl. Phys.* **116**, 163905 (2014).
31. Wang, J. B., Mi, W. B., Wang, L. S. & Peng, D. L. Interfacial-scattering–induced enhancement of the anomalous Hall effect in uniform Fe nanocluster-assembled films. *Europhys. Lett.* **109**, 17012 (2015).
32. Meier, H., Kharitonov, M. Y. & Efetov, K. B. Anomalous Hall effect in granular ferromagnetic metals and effects of weak localization. *Phys. Rev. B* **80**, 045122 (2009).
33. Liu, H., Lee, F. K., Zheng, R. K., Zhang, X. X. & Tsui, O. K. C. Extraordinary Hall effect in $(Ni_{80}Fe_{20})_x(SiO_2)_{1-x}$ thin films. *Phys. Rev. B* **70**, 224431 (2004).
34. Cheng, Y. H., Zheng, R. K., Liu, H., Tian, Y. & Li, Z. Q. Large extraordinary Hall effect and anomalous scaling relations between the Hall and longitudinal conductivities in ε-Fe_3N nanocrystalline films. *Phys. Rev. B* **80**, 174412 (2009).
35. Zhang, Q. *et al.* Anomalous Hall effect in Fe/Au multilayers. *Phys. Rev. B* **94**, 024428 (2016).
36. Wang, J. Q. & Xiao, G. Large finite-size effect of giant magnetoresistance in magnetic granular thin films. *Phys. Rev. B* **51**, 5863 (1995).
37. Chen, J. & Hershfield, S. Effect of spin-flip scattering on current-in-plane giant magnetoresistance. *Phys. Rev. B* **57**, 1097 (1998).
38. Imort, I.-M., Thomas, P., Reiss, G. & Thomas, A. Anomalous Hall effect in the Co-based Heusler compounds Co_2FeSi and Co_2FeAI. *J. Appl. Phys.* **111**, 07D313 (2012).
39. Wang, L. S. *et al.* Gas-phase preparation and size control of Fe nanoparticles. *Appl. Phys. A* **103**, 1015 (2011).

Acknowledgements

This work was partially supported by the National Natural Science Foundation of China (Grant Nos 51371154 and 51571167), the Fundamental Research Funds for the Central Universities (Grant No. 20720140547).

Author Contributions

D.L.P. and L.S.W. initiated the study. Q.F.Z., X.Z.W. and H.F.Z. prepared the samples by plasma-gas-condensation (PGC)-type cluster deposition system. Q.F.Z. and J.X. performed the PPMS-9 measurements. L.L., X.L., Y.L.Q. and Y.Z.C. performed the SEM and TEM measurements. All the authors contributed to discussion of the project.

Additional Information

Supplementary information accompanies this paper at https://doi.org/10.1038/s41598-017-11983-7.

Competing Interests: The authors declare that they have no competing interests.

Publisher's note: Springer Nature remains neutral with regard to jurisdictional claims in published maps and institutional affiliations.